WATER DYNAMICS

4th International Workshop on Water Dynamics

Sendai, Japan *7 - 8 November 2006*

EDITORS
Kazuyuki Tohji
Noriyoshi Tsuchiya
Balachandran Jeyadevan
Tohoku University, Sendai, Japan

SPONSORING ORGANIZATIONS
Graduate School of Environmental Studies
21st Century COE Program, Tohoku University
International COE of Flow Dynamics
Advanced Science and Technology Center for the Dynamic Earth

AMERICAN INSTITUTE OF PHYSICS

Melville, New York, 2007
AIP CONFERENCE PROCEEDINGS ■ VOLUME 898

Morphology Control of FeCo Alloy Particles Synthesized by Polyol Process

D. Kodama[1], K. Shinoda[2], K. Sato[3], Y. Sato[1], K. Tohji[1], and B. Jeyadevan[1]

[1]*Graduate school of Environmental Studies, Tohoku Univ., Sendai, Miyagi 980-8579, Japan;*
[2]*Institute of Multidisciplinary Research for Advanced Materials, Tohoku Univ., Sendai, Miyagi, 980-8577,*
[3]*Dowa Mining Company, Chiyoda, Tokyo 110-8282, Japan*

Abstract. FeCo alloy is a soft magnetic material that possesses the highest saturation magnetization of 2.4 T and crystallizes in bcc structure as in the case of α -Fe. However, the particles synthesized were highly agglomerated. Thus, in this paper, an attempt was made to control the morphology of the particles using different types and concentrations of surfactants such as oleic acid, oleyl amine, polyvinylpyrrolidone (PVP), etc., during the synthesis of the particles. Though all the surfactant experimented partially prevented the agglomeration, products had larger size distribution except for PVP, which provided nearly monodispersed particles. Furthermore, the FeCo particles synthesized in the presence of PVP were either cubic or nearly spherical depending on the concentration of Fe.

Keywords: Polyol process; Fe-Co nanoparticles; Soft magnetic materials
PACS: 74.25.Ha; 75.50.Bb; 75.50.Tt

INTRODUCTION

The bulk FeCo alloy is used in various engineering applications, due to their high saturation magnetization, high Curie temperature, high permeability, low coercivity and anisotropy [1]. On the other hand, though the potential of FeCo nanoparticles in various fields [2] has also been envisaged, they are yet to be explored fully due to unavailability of the same. Though there have been reports attempting the synthesis of FeCo bimetallic alloy particles by polyol process [3] nearly a decade ago, the successful synthesis of oxide-free powders with varying particle sizes and chemical compositions using the modified polyol process was reported by the authors, only recently[4]. It was noted that the basic morphology of the particles were cubic and degree of agglomeration depended on the type and concentration of the surfactant utilized during the synthesis of the same. In this paper, we report the experimental results of the study undertaken to control the morphology of the FeCo alloy nanoparticles utilizing different types of surfactants.

EXPERIMENTAL

In polyol process, the metal salts are dissolved in liquid polyol under an inert atmosphere and heated to elevated temperatures to obtain fine metal or alloy nanoparticles. FeCo alloy nanoparticles were prepared by dissolving $FeCl_2.4H_2O$, Co (acetate)$_2$.$4H_2O$, NaOH and surfactants in 100ml ethylene glycol and heating the solution was up to 403K while stirring. Then, the reaction vessel was refluxed for two hours this temperature. Finally, the suspension was cooled down to RT. The products were recovered from polyol and washed with ethanol. The crystal phase identification, particles size and degree of agglomeration, chemical composition, and magnetic properties of the products were analyzed using X-ray diffraction analysis (XRD), Scanning electron microscope (SEM), X-ray fluorescence (XRF), and vibration sample magnetometer (VSM), respectively.

RESULT AND DISCUSSION

Properties of FeCo Nanoparticles Synthesized by Modified Polyol Process

The successful synthesis of Fe-Co nanoparticles by using a modified polyol process has been already reported [4]. The formation of the alloy nanoparticles was confirmed by X-ray diffraction (Fig. 1) and x-ray extended absorption fine structure analyses. The concentration of iron in these particles could be varied between 40 and 90 percent by controlling the reaction

CP898, *Water Dynamics: 4th International Workshop on Water Dynamics*
edited by K. Tohji, N. Tsuchiya, and B. Jeyadevan

conditions such as initial Fe/Co ratio, reaction temperature and hydroxyl ion concentration. The highest magnetization of 225 emu/g was recorded for $Fe_{70}Co_{30}$ nanoparticles.

Figure 2 shows the SEM image of the (a) $Fe_{75}Co_{35}$, (b) $Fe_{50}Co_{50}$ particles synthesized with and (c) without surfactants. The shape of FeCo particles varied from cubic to nearly spherical when the particles were rich in Fe or Co. The Fe rich FeCo particles take cubic shape, where as the Co rich particles become nearly spherical irrespective of the presence of any surfactants. On the other hand, it should be noted that the degree of agglomeration as well as the particle size and size distribution was reduced when a surfactant was used during the synthesis. Additionally, particle size was also controlled between about 200 nm and 35 nm only through the synthesis in the presence of surfactant. However, the synthesis of particles with diameter less than 35 nm is yet to be achieved. Thus, further investigation was necessary to determine the suitable surfactant to control the degree of agglomeration as well as the particle size distribution, for the use of these particles in various potential applications. Thus, the effect of various surfactants on the morphology and size dispersion of the product and also, the most appropriate surfactant as well as its optimum concentration is investigated and discussed in the next section.

Influence of Surfactant on Particle Size, Size Distribution and Morphology

Generally, the synthesis of monodispersed or size controlled particles are realized with the help of surfactants, which inhibit the growth of the particles and also prevents agglomeration. There are various types of surfactants with head groups such as COO^-, NH_2, SO_3^- and so on. Thus, the synthesis of FeCo nanoparticles was carried out with some of the representative surfactants such as oleyl amine, oleic acid, sodium dodecyl benzene sulfonate, adamantine carboxylic acid and PVP, which are known for its affinity towards oxide, metal or alloy surfaces. And also, the effect of hydrophobic chain length on the properties of the particles was studied by using carbonic acid surfactants whose chain lengths are shorter than that of oleic acid.

Figure 3 shows the SEM image of the FeCo particles synthesized by using oleylamine, oleic acid, sodium dodecyl benzene sulfonate, adamantine carboxylic acid and PVP. In the case of oleylamine, the concentration was not high enough to prevent agglomeration. However, the form of agglomerates were different from the one synthesized in the absence of surfactants and the agglomerates had large flat

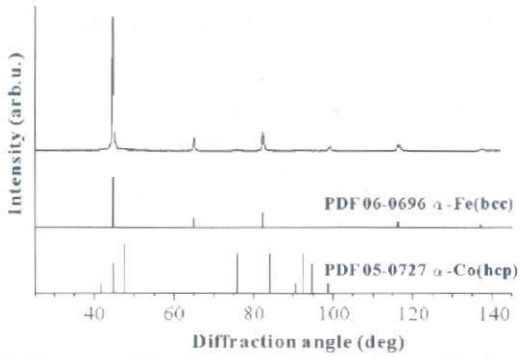

FIGURE 1. XRD pattern of FeCo particles synthesized by modified polyol process.

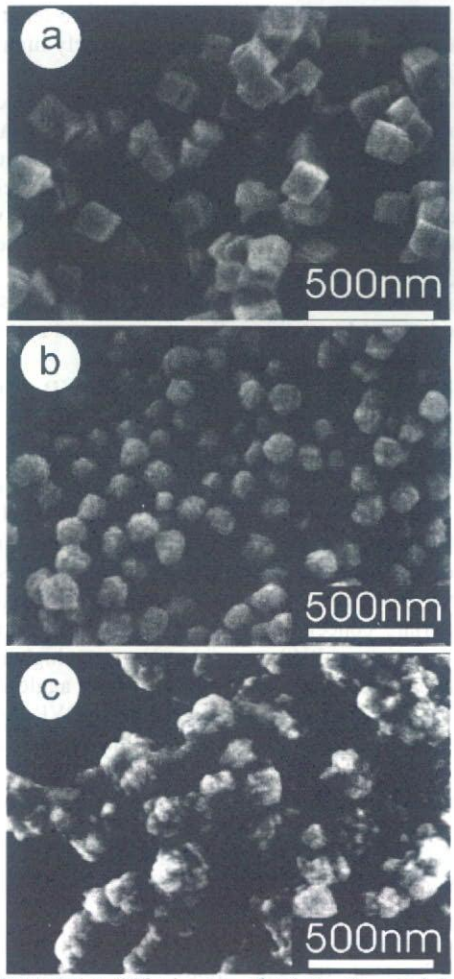

FIGURE 2. SEM images of (a) $Fe_{75}Co_{35}$ and (b) $Fe_{50}Co_{50}$, and $Fe_{75}Co_{35}$ particles synthesized with surfactant, and (c) the FeCo particles prepared in the absence of surfactant.

surface and steps at the corner. This suggested the surfactant-induced variation in particle growth. Furthermore, the agglomerates were consisted of large cubic particles. When the concentration of oleylamine was increased ten times, the particles rather agglomerated, however, it included small sized cubic particles. It should be noted that when the synthesis was carried out with oleylamine, cubic particles about 250 nm were obtained in large numbers compared to the particles synthesized with other surfactants. This result also suggested that controlling the amount of oleylamine, or using the same along with other surfactants may facilitate the formation of larger particles.

The degree of agglomeration of the products synthesized with other surfactants was low. However, the correlation between particle size and molecular length of surfactant was not established. This may be due to the fact that difference between the lengths of surfactant molecules was not comparatively high. The products obtained using surfactants other than PVP had larger size distribution. Additionally, high melting temperature of the surfactants caused material handling problem. For example, when the stearic and lauric acids were used as surfactants, the suspension dispersing FeCo particles become solidified while cooling and consequent process to recover particles get complicated. From the above results, PVP was considered as a suitable surfactant for synthesis of monodispersed particles in this experimental system.

The Synthesis of FeCo using PVP with Different Molecular Weight

The FeCo synthesis experiments were carried out with various concentrations of PVP K-30 (MW = 40,000), ranging from 0.05 to 2.5 mol/l of pyrrolidone monomer. The agglomeration of FeCo particles was inhibited when the concentration of PVP was in the appropriate concentration range. However, when the concentration of PVP was either lower or higher than the allowable range, particles began to agglomerate strongly. The particles synthesized using PVP K-30 of concentration varied between allowable ranges influenced the size appreciably and the smallest particles were obtained when the ratio between PVP K-30 and metal ions was 10.

The experiments were also carried out with various molecular weights of PVP, such as K-16 (MW = 8000), K-90 (MW = 360000) and vinylpyrrolidone, while maintaining the pryrrolidone monomer to metal ion ratio fixed at 10. The approximate size of FeCo particles prepared with PVP K-16, K-90 and vinylpyrrolidone were about 50, 120 and 100 nm, respectively. The above results suggested that the length of PVP molecule has a pronounced influence on FeCo particle sizes and there could be an optimum length and concentration to obtain particles with smaller diameter. Thus, studies related to the synthesis of monodispersed particles with smaller diameter is being attempted by tuning the length and concentration of PVP.

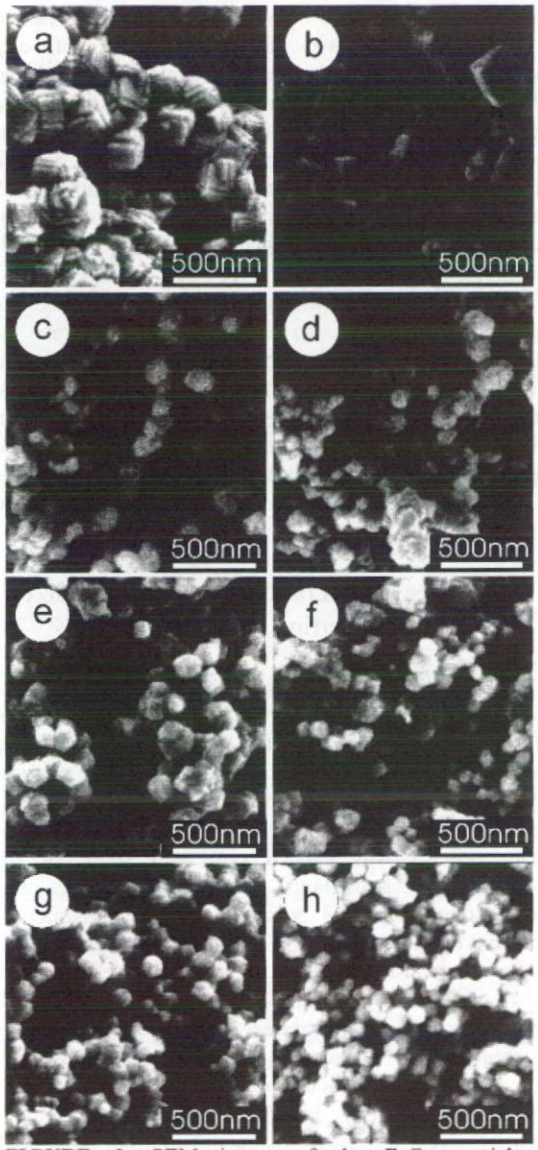

FIGURE 3. SEM image of the FeCo particles synthesized with surfactant (a) oleylamine, surfactant / metal molar ratio (S / M) = 1, (b) oleylamine S / M = 10, (c) oleic acid, (d) stearic acid, (e) lauric acid, (f) adamantine carboxylic acid, (g) sodium dodecyl benzene sulfonate and (h) PVP K-16.

CONCLUSION

The FeCo nanoparticles were synthesized by using surfactants with different head groups. The presence of surfactants during particles formation prevented the agglomeration of the particles and composition dependent morphology became distinct. The FeCo particles rich in iron took the shape a cube, whereas Co rich particles were nearly spherical in shape. Though every surfactant partially prevented the agglomeration, the monodispersity of the particles was observed only in the case of PVP. The results of the study carried out using PVP of different molecular weight suggested the possibilities of synthesizing monodispersed particles with varying sizes.

REFERENCES

1. Y.G. Chin and H.J. Wernich, in: E.P. Wohlfarth (Ed), *Ferromagnetic materials*, North Holland, Amsterdam, 1980.
2. N.H. Duc, T. M. Danh, N. A. Tuan and J. Teillet, *Appl. Phys. Lett.* **78**, 3648-3650 (2001).
3. G. Viau, F. Fievet-Vincent, F. Fievet and *J. Mater. Chem.* **6**, 1047-1071 (1996).
4. D. Kodama, K. Shinoda, K. Sato, Y. Sato, B. Jeyadevan and K. Tohji, *Adv. Mater.* **18**, 3154-3159 (2006).

Magnetite Nanoparticles for Magnetic Fluid Hyperthermia Using Modified Oxidation Method

T. Hosono, H. Takahashi, Y. Sato, K. Tohji, and B. Jeyadevan

Graduate School of Environmental Studies, Tohoku University, 6-6-20 Aoba, Aramaki, Aoba-ku, Sendai, Japan

Abstract. Magnetic fluid hyperthermia (MFH) utilizing the heat generated by the magnetic particles exposed to external AC magnetic field has an edge over the other hyperthermia techniques, since the heat source can be localized in cancer cells with an external magnetic field and their position can be detected by utilizing their magnetic properties. Heating rate depends on the particle diameters and the experimental investigations by using magnetite particles suggested that the optimal size could be above 11nm. Thus, in this paper, a technique to synthesize monodispersed magnetite particles with diameters raging between 11 and 20 nm is reported. Furthermore, a detailed analysis of the relationship between particle size and heating rate is reported based on the magnetic and heat dissipation properties of magnetite particles synthesized by the modified oxidation method.

Keywords: Magnetic fluid hyperthermia, Magnetite, Modified oxidation method
PACS: 78.67.Bf

INTRODUCTION

Magnetic fluid hyperthermia (MFH) is one of the cancer therapy methods that destroy tumors using the heat generated from magnetic particles exposed to an AC magnetic field. Using this method, it is possible to destroy only cancer cells and inhibit the side effects. Recently, MFH on human using magnetite particle suspension has been reported [1]. However the basic information such as optimum particle diameter, concentration, etc are not investigated enough to optimize the treatment conditions and also to reduce the level of risk.

BACKGROUND

Since the heating rate is influenced by the particle diameter and magnetic property, theoretical and experimental investigations have been carried out using magnetite particles of various diameters [2,3]. The theoretical investigation has revealed that the particle with diameters ranging between 11-13 nm is involved in the dissipation of most of the heat. Consequently, magnetite particles of around 11 nm were synthesized by coprecipitation and thermal decomposition method and their magnetic and heating properties were investigated [4]. However the particles synthesized by coprecipitaion method have wide size distribution. Therefore size classification was carried out to remove the particles with diameters less than 8 nm and the sample with average diameter of 14 nm was prepared (sample(a)). The particles synthesized by thermal decomposition had narrow distribution and average diameter was 11 nm (sample(b)). The samples of 3 ml isoparaffin suspension of 4 wt % particle concentration were made using sample(a) and sample(b). Heat generation measurement was conducted on the condition that intensity and frequency of AC magnetic field were 3.2 kA/m and 600 kHz, respectively. The temperature of sample(a) rose up to 100°C within a minute. On the other hand, temperature of sample (b) rose up to only 35°C even after exposing the particles for 10 minutes. Next, blocking temperature measurements were carried out in both DC and AC magnetic fields. Blocking temperature (T_B) of sample(a), was 235 K in DC magnetic field and shifted to more than 300 K in AC magnetic field of 10 kHz. On the other hand T_B of sample(b) was 140 K in DC magnetic field and it shifted to a temperature as high as 180 K in AC magnetic field of 10 kHz [5]. If we correlate the magnetic measurement results with heat dissipation, we could explain their behavior as follows. In the case of sample (a) which indicated high heat dissipation was believed due to a large number of particles whose magnetic relaxation were delayed against AC magnetic field at around 300 K. In the case of sample (b), most

CP898, *Water Dynamics: 4th International Workshop on Water Dynamics*
edited by K. Tohji, N. Tsuchiya, and B. Jeyadevan

of the particles were thermally agitated at around 300K, and either they relax in the magnetic field direction without any delay or does not orient their magnetic vector in the field direction due to higher thermal energy than the magnetic energy. These results suggest that the magnetite particles with their blocking temperature around R.T at 600 kHz are suitable for magnetic hyperthermia.

EXPERIMENTAL

In general, coprecipitation, thermal decomposition and oxidation methods are used to synthesize magnetite particles. The particles synthesized by coprecipitation method have diameters in the rage of 5 to 20 nm with wide size distribution. In thermal decomposition method, it is possible to synthesize monodispersed magnetite particles up to 11nm. But it is very difficult to synthesize particles with diameters more than 11nm. Furthermore, it is also expensive and environmentally unfriendly. On the other hand, particles in the range of sub μm in size with wide size distribution can be synthesized by conventional oxidation method. However, it is possible to synthesize magnetite particles with diameter raging between 11 to 20 nm by controlling the oxidation rate using a modified oxidation method described below.

Synthesis of Magnetite Particles by Oxidation Method

In the conventional oxidation method, the particles are synthesized by adding ferrous ion to a mixture of alkali and oxidant. The particles with diameters of sub μm with wide size distribution are synthesized by conventional oxidation method using only ferrous ion (eq. (1)).

$$Fe^{2+} + \text{oxidant} \rightarrow Fe^{3+}$$
$$Fe^{2+}+2Fe^{3+}+8OH^- \rightarrow Fe(OH)_2+2Fe(OH)_3 \rightarrow Fe_3O_4+4H_2O \quad (1)$$

In this method, nucleation is achieved by the oxidation of ferrous to ferric ion by the oxidant and then these nucleuses grow as the ferrous ions are gradually oxidized to ferric. However, using this method, it is difficult to synthesize magnetite particles raging between 11 to 20 nm due to slow oxidation rate. Furthermore, since there is no clear separation between nucleation and growth steps, the particles become broadly distributed.

Thus, in the modified oxidation method, the particles were synthesized by using a mixture of ferrous and ferric solution. In this method, it is possible to generate rapid nucleation by initiating a reaction similar to coprecipitation by using ferric ion from the beginning (eq. (2)). The rest of the ferrous ion, which does not take part in nucleation, is used to grow the particles (eq. (1)). It is possible to control the number of nucleus by using ferric ion and separate the nucleation and growth steps clearly.

$$Fe^{2+}+2Fe^{3+}+8OH^- \rightarrow Fe(OH)_2+2Fe(OH)_3 \rightarrow Fe_3O_4+4H_2O \quad (2)$$

In this study, reaction temperature is kept constant at 90°C and the initial ferric, NaOH, KNO_3 concentrations and air blowing rate which influence the number of nucleus, aggregation of nucleus and uniform growth of the particles, respectively were varied. Sample A was synthesized with Fe^{3+} initial concentration of 30 mol% and KNO_3 as oxidant. Sample B and C were synthesized with Fe^{3+} initial concentration of 40 mol% and air as oxidant.

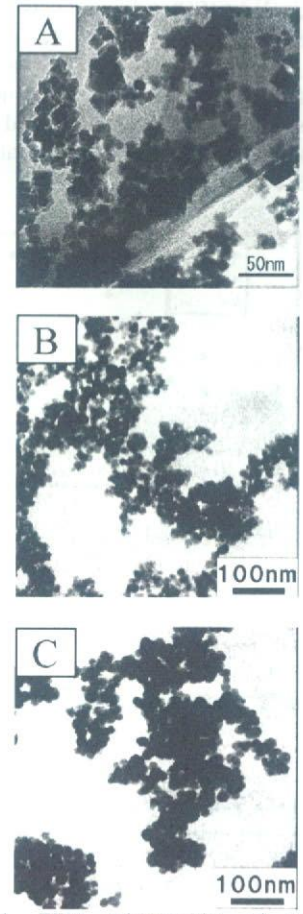

FIGURE 1. TEM micrographs of sample A (Dm=13nm), sample B (Dm=15nm) and sample C (19 nm) synthesized by modified oxidation method.

Characterization

TEM and XRD were used to characterize the morphology and phase of the samples. The average grain diameter was calculated from the Scherrer formula for the particles synthesized by the modified oxidation method.

And the relationship between particle size and heating rate was investigated by exposing a suspensions dispersing magnetite particles of 0.2 g in 2 ml of water was used in this measurement. Measurement conditions were input power 500W, frequency 600 kHz and intensity 3.2 kA/m.

Saturation magnetization and coercivity were recorded using a vibration sample magnetometer (VSM). Blocking temperature measurements were carried out using Superconducting Quantum Interference Device (SQUID). Field cooled (FC) and zero field cooled (ZFC) measurements were conducted at temperatures from 5 to 300 K with an applied magnetic field of 4 kA/m. The variation in the magnetization against temperature is used to project the size distribution of the samples. And the discussion on the relationship between heating rate and particle size was based on these data.

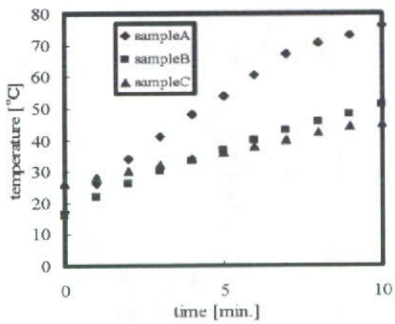

FIGURE 2. Temperature against exposure time of the magnetite suspensions dispersing samples A, B and C exposed to an ac magnetic field. (intensity 3.2 kA/m and frequency 600 kHz)

RESULTS AND DISCUSSION

Characterization of Magnetite Particles

TABLE 1. Magnetic properties of magnetite samples with various average size particles synthesized by modified oxidation method.

	Dm [nm]	Ms [emu/g]	Hc [Oe]
sample A	13	45.6	15.8
sample B	15	63.3	19.0
sample C	19	68.7	38.0

The samples with different mean particle size raging between 11 to 20 nm could be synthesized by the modified oxidation method (Fig. 1). Furthermore grain size calculated with Scherrer formula was almost equal to particle size estimated from the TEM micrographs. Therefore, it can be considered that the particles synthesized by modified oxidation method were single crystal and the average diameters of each samples were 13 (sample A), 15 (sample B) and 19 nm (sample C), respectively. Saturation magnetization and coercivity of samples were as shown in Table 1.

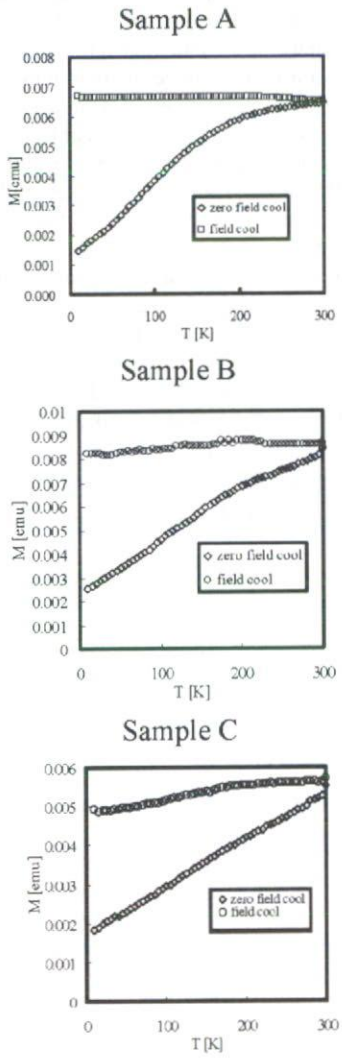

FIGURE 3. Field-cooled and zero field–cooled magnetic measurements against temperature for sample A, B and C.

Heat Generation Measurements

Heat generation measurements were carried out for sample A, B and C (Fig. 2). The samples were exposed to AC magnetic field for 10 minutes. Temperature of sample A, B and C rose up to 76, 51 and 45°C, respectively. The highest heating rate was obtained for the sample A with a mean size of 13 nm and the heat generation decreased with the increase in average particle size.

This result is in accordance with the trend from theoretical calculations. On comparison with previous reports, heating rate for sample A was lower although the mean size was about 13 nm. In order to evaluate the reason for lower heating rate, blocking temperature measurements were made.

Blocking Temperature Measurements

Blocking temperature (TB) measurements from the FC and ZFC data of each samples were made using SQUID (Fig. 3). TB is estimated from the temperature at which the FC and ZFC meet. TB of Sample A is about 300 K. But TB of samples B and C are more than 300 K. TB increased with the increase in average particle diameter. In previous reports, it was revealed that magnetization of samples with wide size distribution varied slightly against temperature. Since magnetization of each sample varied only slightly against temperature, it indicates that the samples consist of large particles and have broad size distribution and/or the particle-particle magnetic interaction becomes higher with increasing particle diameter. As a consequence the blocking temperatures also become higher. Therefore, it can be imagined that TB might be shifted to much higher temperature in AC magnetic field of 600 kHz. Therefore, to minimize the interaction as well as the shift in the blocking temperature, further effort is necessary to improve the particle synthesis technique to enable the preparation of particle with much narrower size distribution and less sensitive to frequency variations.

CONCLUSION

Magnetite particles with different mean size were synthesized by a modified oxidation method. It was found that each sample had wide size distribution from the TEM and SQUID measurements. Sample A indicated higher heat generation and T_B of 300 K. However it is necessary to synthesize the particles with a very narrow size distribution to analyze the relationship between particle size and heating rate in detail. Furthermore it is also necessary to investigate modified oxidation method to synthesize monodispersed particles.

REFERENCES

1. M. Johannsen, U. Gneveckow, L. Eckelt, A. Feussner, N. Waldofner, R. Scholz, S. Deger, P. Wust, S.A. Loening and A. Jordan, *Int. J. Hyperthermia* **21**, 637-647 (2005).
2. R.E. Rosensweig, *J. Magn. Magn. Mater.* **252**, 370-374 (2002).
3. T. Atsumi, B. Jeyadevan et al., *J. Magn. Soc. Jpn.* **30**, 555-560 (2006).
4. T. Atsumi, B.Jeyadevan et al., *J. Magn. Magn. Mater.* (in press)
5. T. Atsumi, B.Jeyadevan et al., *J. Magn. Soc. Jpn.* (in press)

Evaluation of Multi-Walled Carbon Nanotube Scaffolds for Osteoblast Growth

N. Tsuchiya [a], Y. Sato [a,*], N. Aoki [b], A. Yokoyama [b], F. Watari [b], K. Motomiya [a], B. Jeyadevan [a], and K. Tohji [a]

[a] *Graduate School of Environmental Studies, Tohoku University, Aoba 6-6-20, Aramaki, Aoba-ku, Sendai, 980-8579, Japan*

[b] *Graduate School of Dental Medicine, Hokkaido University, Kita 13, Nishi 7, Kita-ku, Sapporo, 060-8586, Japan*

Abstract. The development of carbon nanotubes (CNTs) for tissue engineering and regenerative medicine has attracted a great deal of attention. Multi-walled carbon nanotube (MWCNT) scaffolds have been used for the successful proliferation of osteoblasts. In this study, osteoblast cells were cultured on prepared scaffolds *in vitro* and the characteristics of each scaffold were evaluated in an effort to investigate the effect of surface properties such as roughness and the adsorption of albumin on MWCNT scaffolds with different diameters.

Keywords: Multi-walled carbon nanotubes, Osteoblast, Scaffolds, Cell proliferation, Wettability, Roughness, TGF-β1
PACS: 42.62.Be, 47.54.Fj

INTRODUCTION

Carbon nanotubes (CNTs) have attracted a great deal of attention because of their unique properties, such as extreme mechanical strength, large aspect ratio and relatively large specific surface area. Many researchers have been investigating applications of CNTs in various fields. Our recent studies employing *in vitro* and *in vivo* experiments showed that CNTs were low in toxicity, at least in the short term [1], and exhibited excellent properties for use as scaffolds in cell cultures [2].

However, no study has investigated factors necessary for effective cell growth on CNT scaffolds. The mechanism of cell growth on scaffolds is generally considered as follows: A) water molecules and ions are physically adsorbed onto the surface of scaffold materials, B) proteins are then adsorbed on the surface of the water molecules and/or ions, C) cells come in contact with the adsorbed layers of proteins, and D) cells finally bond with the scaffold materials through the cytadherence protein layer and proliferate, as shown in Fig. 1. This mechanism suggests that surface conditions (surface area, roughness, surface charge, surface wettability, etc.) may influence cell growth. In addition, proteins play an important role in facilitating cell adhesion onto the scaffolds.

We have been investigating cell proliferation of osteoblasts (bone-forming cells) cultured on multi-walled carbon nanotube (MWCNT) scaffolds and the surface properties of these scaffolds. In this study, we focused on physicochemical properties of MWCNT scaffolds (surface roughness and adsorption of albumin) in relation to osteoblast proliferation.

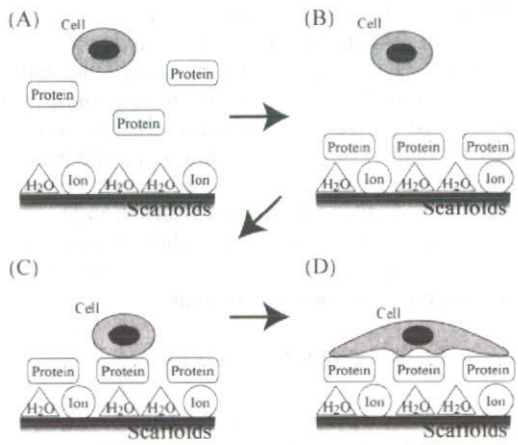

FIGURE 1. Scheme of the passage of time until cells in culture adhered onto scaffolds.

*To whom correspondence should be addressed. E-mail: hige@bucky1.kankyo.tohoku.ac.jp

CP898, *Water Dynamics: 4th International Workshop on Water Dynamics*
edited by K. Tohji, N. Tsuchiya, and B. Jeyadevan

EXPERIMENTAL DETAILS

Substrate Materials

We chose MWCNTs with different diameters, 10 nm and 200 nm, and refer to these forms as "MW10" and "MW200", respectively. We also prepared graphite (Gr) with a size of 7.5 μm, which was the same size as the carbon materials. Polycarbonate (PC) and polystyrene (PS) were used as reference samples.

Preparation of Scaffolds

MWCNTs and graphite were prepared using sonication in a mixture of concentrated H_2SO_4 and HNO_3 in the ratio 3:1 for 5 hrs. These samples were well dispersed in water. Using these samples, scaffolds were prepared as follows: a prescript quantity of CNT or graphite (see Table 1) was dispersed in 100 mL of deionized water by sonication. Scaffolds were made by suction filtration of the dispersed CNT or graphite slurry onto polycarbonate membranes. After filtration, scaffolds were dried for 3 hrs at 333 K.

TABLE 1. Conditions of prepared scaffolds.

	Weight of samples (mg)	Volume of picking up (mL)
MW10	10	3
MW200	10	8
Graphite	30	5

Physicochemical Properties

Contact angles of the surface of scaffolds were measured in order to obtain a measure of wettability. Each sample was soaked in deionized water or PBS(-) for 1 day and the contact angle was determined after drying. The contact angle was measured in a solid-gas-liquid system due to the mesh-like structures of MWCNT scaffolds.

Surface roughness was determined using a surface roughness measuring device.

We used albumin (from human serum) in an effort to measure adsorption of proteins because albumin is a constituent of the bone matrix. Each sample was soaked in 5 mL of a 10 mg/L albumin/PBS(-) solution and incubated for 4 hrs under a real cell incubation environment. Albumin was desorbed after incubation using a 1% SDS solution, which is a kind of surfactant. After the desorption process, adsorption of albumin was determined using a BCA assay.

Cell Culture

We cultured osteoblasts as follows: 1.0×10^5 human osteoblast-like cells (Saos2 cells) were seeded on each scaffold, and the cells were cultured in Dulbecco's modified Eagle's medium (DMEM) containing 10% fetal bovine serum (FBS) and 1% penicillin/streptomycin under standard cell culture conditions (at 310 K in a humidified 5% CO_2/ 95% air environment) for 3 days and 7 days. After the prescribed time period, cell proliferation and morphology were investigated using a scanning electron microscope (SEM).

Immunoassay

Transforming growth factor-β1 (TGF-β1) is one of the cytokines that work in the early stage of osteoblast growth, and gives an indication of whether cells have grown normally. The concentration of TGF-β1 in the culture medium after cell culture was determined using Quantikine Human TGF-β1 kits (R&D systems).

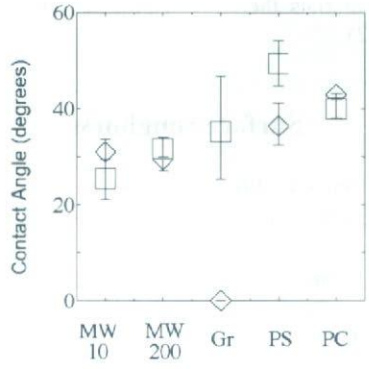

FIGURE 2. Contact angle of the surface of each scaffold material. □: soaked in deionized water and ◇:soaked in PBS(-).

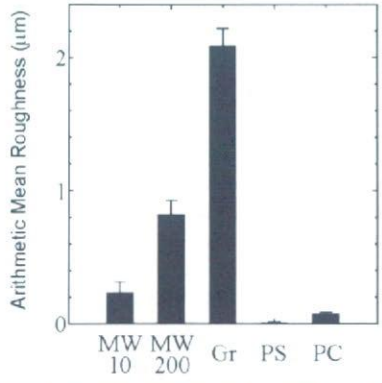

FIGURE 3. Surface roughness of each scaffold material.

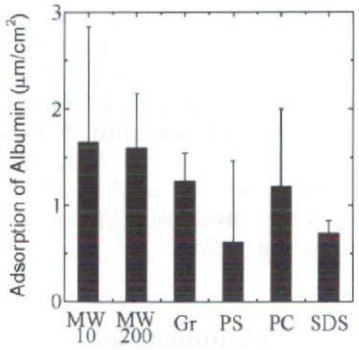

FIGURE 4. Adsorption of albumin of each scaffold material.

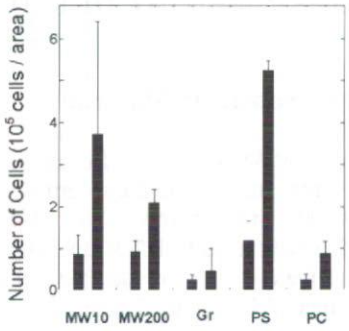

FIGURE 5. Total number of cells on scaffolds. The bars on the left and right represent the culture for 3 and 7 days, respectively.

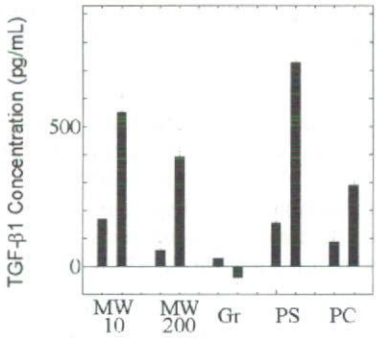

FIGURE 6. TGF-β1 concentration of each scaffold. The bars on the left and right represent the culture for 3 and 7 days, respectively.

RESULTS

Wettability

The relative contact angles of each sample were as follows: Gr < MW200 ≒ MW10 < PC ≒ PS. The carbon materials therefore exhibited high wettability (see Fig. 2).

Surface roughness

The relative surface roughness of each sample was as follows: PC ≒ PS < MW10 < MW200 < Gr (Fig. 3). Carbon materials have a much higher roughness than PC or PS scaffolds. However, the range of roughness was not in the order of nanometers, but micrometers.

Adsorption of Albumin

MWCNT scaffolds exhibited a high adsorption of albumin (Fig. 4). In contrast, PS scaffolds did not adsorb albumin.

Cell Proliferation

SEM observations of cultured cells revealed that they formed three characteristic shapes (ball, star and disk) that depended on the properties of the scaffold materials. Furthermore, although cells cultured on MW10 and PS scaffolds for 7 days grew well, it was difficult to determine the shape of such cells (Fig. 5). This result corresponds to TGF-β1 concentrations (Fig. 6). In addition, there was a good association between the number and area of cells on the scaffold.

DISCUSSION

K. L. Elias *et al.* reported that cells grew with an increase in nano-sized surface roughness [3] and that adsorption of protein played a very important role for cell adhesion. Thus, from the physicochemical point of view, carbon materials confer advantages for cell growth. The relative growth of cultured cells on each scaffold was as follows: PC ≒ Gr < MW200 < MW10 < PS. We will now summarize and discuss cell proliferation on each scaffold in relation to physicochemical properties.

Gr scaffolds: Graphite scaffolds had a high wettability and low adsorption of albumin. As cells could not adhere onto Gr scaffolds, they could not grow.

MW10 vs. MW200 scaffolds: both MW scaffolds showed the same amount of adsorption of albumin. MW200 has an advantage for cell growth because of its high surface roughness. In fact, cells grew well on MW10 scaffolds. These results indicated that MWCNT scaffolds with a small diameter are effective for osteoblast growth.

PS vs. PC scaffolds: PS and PC possessed almost the same physicochemical properties. However, cells on PS scaffolds grew much more than those on PC scaffolds.

MW10 vs. PS scaffolds: although MW10 showed a higher adsorption of albumin and larger surface roughness than PS, cells grew well on PS scaffolds.

These results indicated that some other factors not considered in this report affect cell growth, such as functional groups on scaffolds, surface charge, surface energy, and nano-sized surface roughness.

CONCLUSIONS

We investigated cell proliferation from the physicochemical point of view, and found that physicochemical properties and other factors affected cell growth. MWCNT scaffolds exhibit great potential for ostcoblast cell growth.

ACKNOWLEDGMENTS

This work was supported by a Grant-in-Aid for Basic Research No. (S) 14103016 from the Ministry of Education, Science, Culture and Sport of Japan, Grant No. H18-chemistry-006 from Health and Labor Sciences Research Grants from the Ministry of Health, Labor and Welfare, Tohoku University 21st Century COE Program "International COE of Flow Dynamics", Arai Science and Technology Foundation, and the Collaborative Research facility from the Center for Interdisciplinary Research, Tohoku University.

REFERENCES

1. Y. Sato, A. Yokoyama, K. –I. Shibata, Y. Akimoto, S. –I. Ogino, Y. Nodasaka, T. Kohgo, K. Tamura, T. Akasaka, M. Uo, K. Motomiya, B. Jeyadevan, M. Ishiguro, R. Hatakeyama, F. Watari and K. Tohji, *Mol. BioSyst.*, **1**, 176-182 (2005).
2. N. Aoki, A. Yokoyama, Y. Nodasaka, T. Akasaka, M. Uo, Y. Sato, K. Tohji and F. Watari, *J. Biomed. Nanotechnol.*, **1**, 402-405 (2005).
3. K. L. Elias, R. L. Price and T. J. Webster, *Biomaterials*, **23**, 3279-3287 (2000).

Estimation of the Number of Cross-Links of Multi-walled Carbon Nanotube Films Formed by a Dehydration Condensation Reaction

S. Ogino[1], Y. Sato[1], G. Yamamoto[1], K. Sasamori[2], H. Kimura[2], T. Hashida[3], K. Motomiiya[1], B. Jeyadevan[1], and K. Tohji[1]

[1] *Graduate School of Environmental Studies, Tohoku University, 6-6-20 Aoba, Aramaki, Aoba-ku, Sendai 980-8579, Japan*

[2] *Institute for Materials Research, Tohoku University, 2-1-1 Katahira, Aoba-ku, Sendai 980-8577, Japan*

[3] *Fracture and Reliability Research Institute, Tohoku University, 6-6-11-707 Aoba, Aramaki, Aoba-ku, Sendai 980-8579, Japan*

Abstract. Preparation procedure of multi-walled carbon nanotube (MWCNT) films shows as follows. First, as-grown MWCNTs heated in the air and treated with hydrochloric acid to remove amorphous carbon and catalytic metal particles respectively. Then, the obtained MWCNT samples were treated with nitric acid at 373K to add carboxylic acid and hydroxyl groups on their surface. Finally, MWCNT films were prepared by employing a condensation reaction utilizing 1,3-dicyclohexylcarbodiimide (DCC) to cross-link each MWCNT with chemical bonds. Morphological changes in the resultant MWCNT films were monitored using scanning electron microscopy, and showed that the MWCNTs were randomly intertwined in the films. The prepared MWCNT films were 17mm in diameter and 20μm in thickness, and the apparent density was 0.59 g/cm^3. Fourier transform-infrared spectroscopy confirmed that each MWCNT modified with carboxylic acid and hydroxyl groups was cross-linked through the ester bond. It was found that the ratio of the number of ester cross-links and carbon atoms of the nanotubes per unit apparent volume (cm^3) of condensed-MWCNT films was 5.23×10^{-3} using TGA. The tensile strength and Vickers hardness of condensed-MWCNT films achieved an average of 15MPa and 9.2MPa, respectively, and was greater than those of free-standing MWCNT films without ester bond.

Keywords: Multi-walled carbon nanotube, Cross-links, Dehydration, Condensation, Mechanical properties
PACS: 78.67.Ch

INTRODUCTION

Carbon nanotubes (CNTs) films have been utilized in the form of sensor electrodes [1] and actuators [2]. Multi-walled carbon nanotubes (MWCNTs) possess metallic properties and high mechanical strength. However, it is difficult to form MWCNT films since MWCNTs are rigid due to the large number of concentric graphene tubes. To date, researchers have reported on the chemical polymerization of short carboxylic single-walled carbon nanotubes (SWCNTs) into "rings" [3] or "large strands" [4] by application of a condensation reaction. Ester bonds can be synthesized by a dehydration condensation reaction of a carboxylic group with a hydroxyl group in the presence of a dehydration-condensation-coupling agent. In this study, we report on the ester-cross linking of MWCNTs into thin films by employing a dehydration condensation reaction (esterification) with the assistance of 1,3-dicyclohexylcarbodiimide (DCC), and estimate the number of ester cross-links involving MWCNTs and examine the mechanical properties such as tensile strength and Vickers hardness.

EXPERIMENTAL

The MWCNTs used in this study had been synthesized by the CVD method and were obtained from Nanolab, Inc.(as-grown MWCNTs). As-grown MWCNTs heated in the air and treated with hydrochloric acid to remove amorphous carbon and metal particles respectively (purified-MWCNTs). Then, the purified-MWCNTs were treated with nitric acid at 373 K to add carboxylic acid and hydroxyl groups on their surface [5,6]. The resultant sample, referred to as "hydrophile-MWCNTs". The method employed to generate the MWCNT films was as follows: hydrophile-MWCNTs was introduced into a flask

CP898, *Water Dynamics: 4th International Workshop on Water Dynamics*
edited by K. Tohji, N. Tsuchiya, and B. Jeyadevan

containing N,N-dimethylformamide (DMF) and sonicated for 60 min. Following this, the suspension was stirred at room temperature for 24 hours to effectively disperse the nanotubes. 20 ml of the resultant suspension was removed and filtered using a PTFE membrane filter. After filtering the suspension, the cake was thoroughly washed with ethanol to remove DMF. The cake adhered to the PTFE membrane was then sandwiched between Teflon plates and dried at room temperature for over 12 hours under pressure. The resultant sample, referred to as "hydrophile-MWCNT film", was then removed from the PTFE membrane. The method employed to generate MWCNT films assembled by a condensation reaction was as follows: hydrophile-MWCNT films were placed on the Teflon plate inset at the base of a glass petri dish. 20 ml DMF in which 20 mg DCC was added was gently poured into the dish. The dish was then sealed in the flask placed in a water bath set at 333 K, and the reaction allowed to proceed for 24 hours. Following this, DMF was removed from the dish, and DCC and DMF were thoroughly removed using ethanol. The sample was allowed to dry at room temperature for over 24 hours and the resultant film was referred to as "condensed-MWCNT film". The sample was characterized using scanning electron microscopy (SEM), transmission electron microscopy (TEM), Fourier transform-infrared spectroscopy (FT-IR) and high resolution thermogravimetric analysis (TGA). The tensile mechanical properties of MWCNT films were determined using INSTRON 4310.

RESULTS AND DISCUSSION

An image of a condensed-MWCNT film and a typical SEM photograph of its surface are shown in Fig. 1. The condensed-MWCNT films were 17 mm in diameter and 20 μm in thickness (Fig. 1a). Although films were somewhat brittle, they could fashion into various shapes. The hydrophile-MWCNTs possessed an average length 1.5 μm with a curved shape and each MWCNT randomly intertwined in the condensed-MWCNT films (Fig. 1b).

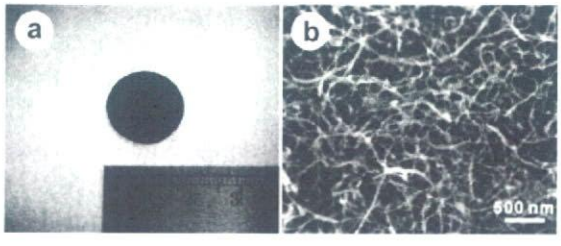

FIGURE 1. (a) Typical image of condensed-MWCNT films. (b) SEM image of the surface of condenced-MWCNT films.

Characterization of the MWCNT films

FT-IR Spectroscopy

The presence of functional groups on the samples was established using IR spectroscopy with transmission method (KBr pellet). From the IR spectra of the hydrophile-MWCNT films and condensed-MWCNT films (Fig. 2), the band present at 1584 cm^{-1} in the two spectra is associated with the stretching vibration of the aromatic C=C group [7]. The half maximum full-width of the broader peak at 1221 cm^{-1} is narrow, and may be accounted for the presence of stretching vibrational modes of ester groups (O-C-O). The 1725 cm^{-1} peak comprises unreacted carboxylic acids and ketones in condensed-MWCNT films, the stretching vibration of the C=O moiety in ester groups (C=O(-O)-C) is thought to be represented by this peak.

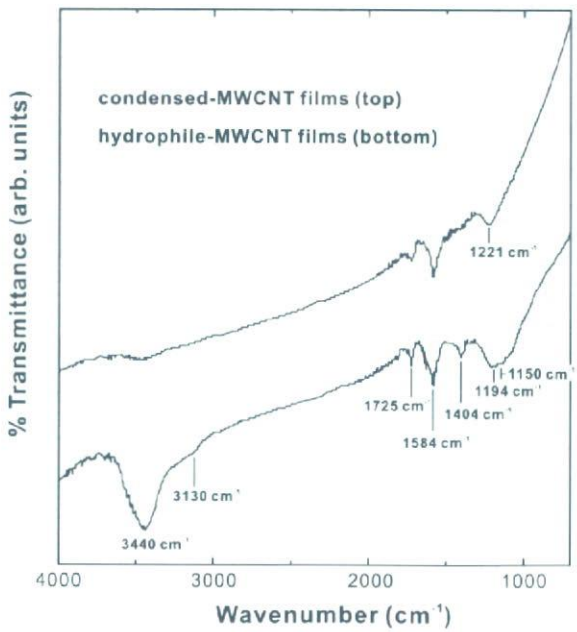

FIGURE 2. FT-IR spectra of condensed-MWCNT films (top), and hydrophile-MWCNT films (bottom).

TG-Mass Analysis

The degree of functionalization has been determined by TG-Mass from 303 K to 1173 K under a helium gas flow. As water in the samples was vaporized *in vacuo* (10^{-3} torr) at 333K for over 12 hours prior to TG-Mass analysis, water molecules were not observed. The generation of CO_2 (m/z 44) was confirmed around 473 K and between 773 and

1073 K for both samples (Fig. 3). According to other studies on activated carbon and carbon nanofibers [8] with oxygen surface groups [7], the maxima on the CO_2 profile are due to the decomposition of carboxylic groups. In the same way, the generation of CO_2 from the nanotube films is attributed to the decomposition of carboxylic acid, ester, lactones and carbonyl groups under a helium gas flow at less than 1073K. In the same range from 473 to 673 K, the amount of CO_2 gas generated from hydrophile-MWCNT films was marked at 500K (Fig. 3a). On the other hand, the amount of CO_2 gas generated from condensed-MWCNT films was marked at 515 and 623 K (Fig. 3b). Condensed-MWCNT films showed a new CO_2-generating maximum at 623 K, in sharp contrast to that of hydrophile-MWCNT films, which might be due to the decomposition of ester bonds. We consider that the difference in temperature associated with the generated CO_2 is dependent on the functional groups (here, ester groups) and the nanotube surface site (end or body of the nanotube) that the functional groups are bonded to, and where the decomposition energy of carboxylic groups and derivatives into CO_2 differs. Although CO gas was confirmed between 573 and 1073 K for both samples, the generated CO gas was very low.

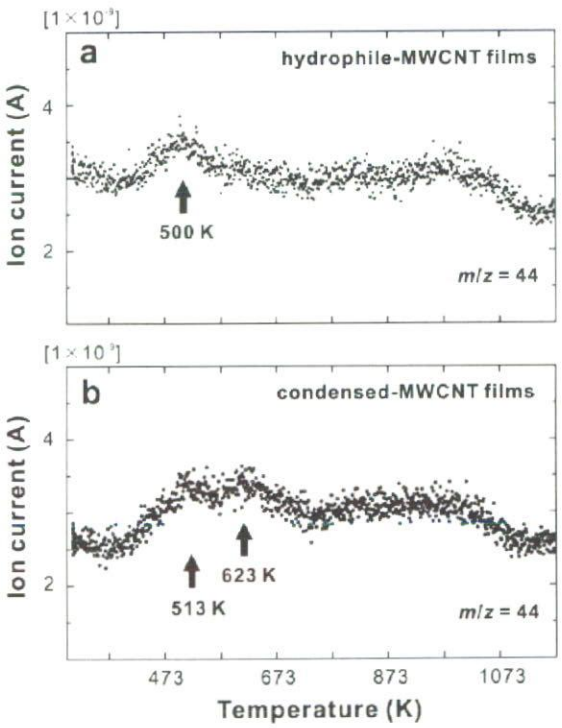

FIGURE 3. Generation of CO2 (m/z 44) of (a) hydrophile-MWCNT and (b) condensed-MWCNT films in a helium atmosphere.

Estimation of the Number of Cross Links of MWCNTs

The typical weight loss for the hydrophile-MWCNT films and condensed-MWCNT films up to 1173 K was approximately 12.2 wt% and 11.5 wt%, respectively (Fig. 4). As water is produced by the dehydration condensation reaction, the difference in weight loss percentage of both films is represented by the ratio of water produced. As the difference in weight loss percentage between hydrophile-MWCNT and condensed-MWCNT films by 1173 K is essentially a weight percentage of the water molecules generated, the molar (X) of the water molecules generated is as follows:

$$X = \left[\left(W_h - W_{cond}\right) \times M_{total}\right] / 1800 \text{ (mol)} \quad (1)$$

Here, W_h is 12.2 wt% of weight loss percentage for the hydrophile-MWCNT films at 1173 K and W_{cond} is 11.5 wt% of weight loss percentage for the condensed-MWCNT films at 1173 K. M_{total} is the total weight of the films. As the apparent density of both samples is 0.59 g/cm^3, the molar of the water molecules generated per unit apparent volume (cm^3) of MWCNT films is 2.29×10^{-4} mol/cm^3. Assuming that ester bonds are uniformly formed all over the condensed-MWCNT films, as a water molecule is produced and an ester bond is formed, the number of ester cross-links formed per unit apparent volume of condensed-MWCNT films is 1.37×10^{20} bond/cm^3.

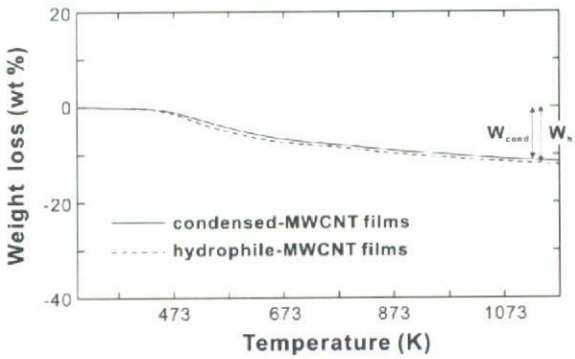

FIGURE 4. TG curves of hydrophile-MWCNT (dashed line) and condensed-MWCNT (solid line) films. W_h and W_{cond} represent the decreasing weight percentage of hydrophile-MWCNT and condensed-MWCNT films, respectively, at 1173K.

TABLE 1. Mechanical properties of hydrophile-MWCNT and condensed-MWCNT films.

	Apparent density (g/cm^3)	Tensile yield strength (MPa)	Elongation to break (%)	Vickers hardness (MPa)	Number of cross links (g/cm^3)
Hydrophile-MWCNT films	0.59	4.8 ± 2.6	6.0 ± 1.5	4.9 ± 0.2	-
Condensed-MWCNT films	0.59	15 ± 5.2	4.5 ± 1.1	9.2 ± 1.3	1.36×10^{20} bond/cm^3

References Mechanical Properties of the MWCNT Films

The tensile stress-strain curve of the condensed-MWCNT and hydrophile-MWCNT films are shown in Fig. 5. The tensile stress-strain curve of condensed-MWCNT films reflects brittle fracture behavior. The tensile measurement of condensed-MWCNT films revealed that the tensile strength to break value was 15 MPa on average, three times stronger than that associated with the hydrophile-MWCNT films (Table 1).

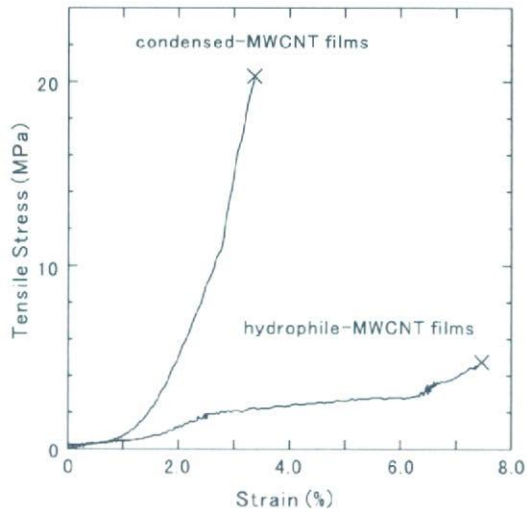

FIGURE 5. Tensile stress-strain curves of hydrophile-MWCNT and condensed-MWCNT films.

CONCLUSIONS

In summary, confirmation that MWCNT films cross-linked through ester bonds was prepared by a condensation reaction in the presence of DCC. Assuming that the ester bonds are uniformly formed all over the condensed-MWCNT films. The tensile strength of condensed-MWCNT films achieved an average of 15 MPa, and is 3.1 times in comparison to those of hydrophile-MWCNT films. The mechanical properties of condensed-MWCNT films might be significantly improved through a condensation reaction by making improvements in ester cross-linking such as chemical modifications with a large number of carboxylic acid and hydroxyl groups thereby increasing the amount of condensation through dense contacts between each carbon nanotube.

REFERENCES

1. R. H. Baughman, C. Cui, A. A. Zakhidov, Z. Iqbal, J. N. Barisci, G. M. Spinks, G. G. Wallace, A. Mazzoldi, D. De Rossi, A. G. Rinzler, O. Jaschinski, S. Roth, M. Kertesz, *Science* **284**, 1340 (1999).
2. J. Kong, M. G. Chapline, H. Dai, *Adv. Mater* **13**, 1384 (2001).
3. M. Sano, A. Kamino, J. Okamura, S. Shinkai, *Science* **293**, 1299 (2001).
4. X. Li, J. Zhang, Q. Li, H. Li, Z. Li, *Carbon* **41**, 598 (2003).
5. M. A. Hamon, J. Chen, H. Hu, Y. Chen, M. E. Itkis, A . M. Rao, P. C. Eklund, R. C. Haddon, *Adv. Matr.* **11**, 834 (1999).
6. Y. H. Li, C. Xu, B. Wei, X. Zhang, M. Zheng, D. Wu, P. M. Ajayan, *Chem. Mater.* **14**, 483 (2001).
7. T. G. Ros, A. J. van Dillen, J. W. Geus, D. C. Koningsberger, *Chem. Eur. J.* **8**, 1151 (2002).
8. Y. Otake, R.B. Jenkins, *Carbon.* **31**, 109 (1993).

Preparation of Size-Controlled Hat-Stacked Carbon Nanofibers

Y. Sato [a], A. Yokoyama [b], K. Motomiya [a], B. Jeyadevan [a], and K. Tohji [a]

[a] *Graduate School of Environmental Studies, Tohoku University, Aoba 6-6-20, Aramaki, Aoba-ku, Sendai, 980-8579, Japan*

[b] *Graduate School of Dental Medicine, Hokkaido University, Kita 13, Nishi 7, Kita-ku, Sapporo, 060-8586, Japan*

Abstract. Hat-stacked carbon nanofibers (H-CNFs) were size-separated using a multi-step microfiltration process employing polycarbonate membrane filters with respective cylindrical pore diameters of 2.0, 1.2 and 0.4 μm after being cut and dispersed in distilled water using sonication in a mixture of concentrated H_2SO_4 and HNO_3. The average length of separated H-CNFs was 2.4 μm, 1.2 μm and 0.6 μm, respectively.

Keywords: Carbon nanofibers, Size control, Tissue response, Toxicity, Inflammatory
PACS: 42.62.Be, 47.54.Fj, 87.19.St

INTRODUCTION

Increasing efforts have been made recently to identify the cytotoxicity of carbon nanomaterials such as C_{60} [1], single-walled carbon nanotubes (SWCNTs) [2-4], multi-walled carbon nanotubes (MWCNTs) [5-7], carbon nanotubes doped with nitrogen [8], and carbon nanofibers [9]. Yokoyama *et al.* evaluated the toxicity of hat-stacked carbon nanofibers (H-CNFs) implanted in the subcutaneous tissue of rats. Granulomatous inflammatory changes were observed around H-CNFs after 1 week and fibrous connective tissue after 4 weeks. However, the absence of necrosis or invasion of neutrophils led the authors to conclude that the wound healing capacity of the tissue was not inhibited and that the carbon nanofibers were not acutely toxic in the subcutaneous tissue of rats. H-CNFs were also observed in phagocytes (arrow A in Fig. 1) 4 weeks after implantation, and were shorter than those observed at 1 week. Some H-CNFs also appeared translucent (arrow B in Fig. 1), a condition that was not observed at 1 week. Unfortunately, the length of H-CNFs implanted in rats was not size-controlled at that point in time. In an effort to confirm the change in length of H-CNFs *in vivo*, size-controlled lengths of H-CNFs are required for use as implanting samples. In this study, we report that H-CNFs were simply cut and dispersed in distilled water using sonication in a mixture of concentrated H_2SO_4 and HNO_3, and size-separated using a multi-step microfiltration process.

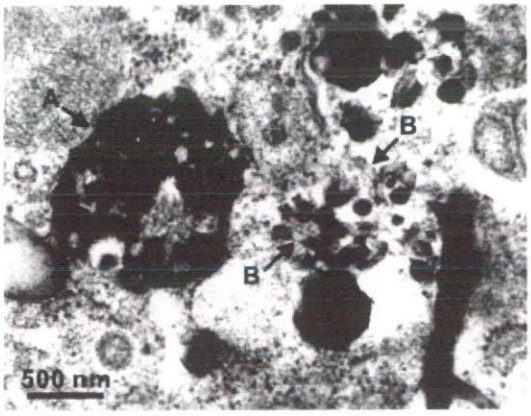

FIGURE 1. TEM images of H-CNFs implanted in subcutaneous tissue at 4 weeks. H-CNFs were observed in phagocytes (arrow A). Some H-CNFs (arrow B) became translucent.

EXPERIMENTAL DETAILS

H-CNFs were produced by thermal CVD using a powdered Ni catalyst in a conventional flow reactor

*To whom correspondence should be addressed. E-mail: hige@bucky1.kankyo.tohoku.ac.jp

CP898, *Water Dynamics: 4th International Workshop on Water Dynamics*
edited by K. Tohji, N. Tsuchiya, and B. Jeyadevan

system according to the report of N. M. Rodriguez [10]. The details of the production methods for H-CNFs were described in a previous report [9]. The structure of H-CNFs resembled the form of bamboo hats stacked upwards toward a needle axis. H-CNFs were heated at 773 K for 60 min under atmospheric pressure. The product was then transferred into a flask with 1.0 L of 6M-HCl and treated at 333 K for 12 hrs to remove nickel and nickel oxides. The acid solution was then filtered using a PTFE membrane filter. The filtered cake was transferred into a flask with 1.0 L of 6M-HNO_3 and refluxed at 373 K for 3 hrs to dissolve the residue nickel. The H-CNFs were then recovered by filtering the suspension with a membrane filter, and the filtered cake was rinsed out with distilled water.

The cutting procedure for purified H-CNFs was as follows: 100 mg of purified H-CNFs was suspended in 100 mL of a 3:1 (v/v%) mixture of concentrated H_2SO_4 (95%) / HNO_3 (60%) and exposed to ultrasonic irradiation for 4 hrs. The resultant suspension was filtered using a membrane filter, and the filtered cake was rinsed out with distilled water. Twenty milligrams of the cut H-CNFs was then suspended in 400 mL of ethanol and irradiated with ultrasonic waves for 1 hr. The cut H-CNFs in the supernatant were then size-separated using a multi-step microfiltration process employing polycarbonate membrane filters with respective cylindrical pore diameters of 2.0, 1.2 and 0.4 μm. Each filtered cake sample was dried *in vacuo* at 373 K for 24 hrs. The sample was characterized using a scanning electron microscope (SEM; S-4100, Hitachi, Japan), a transmission electron microscope (TEM; HF-2000, Hitachi, Japan), inductively coupled plasma optical emission spectrometry (ICP-OES; Thermo Elemental Co. Ltd., USA), Fourier transform-infrared spectroscopy (FT-IR; Avatar 360, Thermo elemental Co. Ltd., USA), and ultraviolet-visible absorption spectroscopy (UV-VIS; U-3300, Hitachi, Japan).

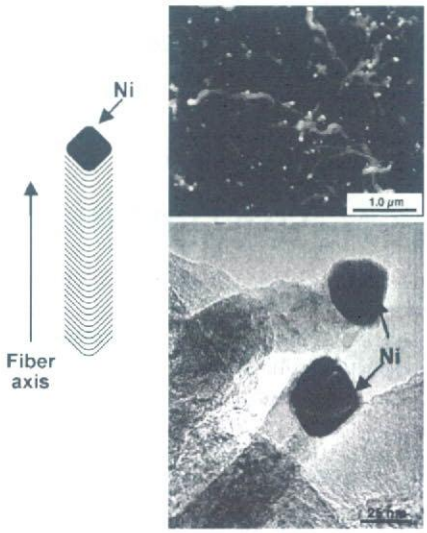

FIGURE 2. Illustration, (a) SEM and (b) TEM images of as-grown H-CNFs.

RESULTS AND DISCUSSION

H-CNFs consisted of curved carbon nanofibers composed of graphene-hats stacked toward a needle axis (Fig. 2). H-CNFs have a diameter of 25–100 nm and a length of 100 nm to 5.0 μm. Although the elemental composition of as-grown H-CNF soot consisted of C: 94.23 wt% and Ni: 5.77 wt% from ICP-OES, the cut H-CNFs consisted of C: 100.00 wt% and were highly pure.

Figure 3 shows IR spectra of as-grown, purified, and acid-sonicated H-CNFs. The band at 1584 cm^{-1} in both spectra was assigned to the stretching vibration of aromatic C=C. The bands around 1398 cm^{-1} and 1240 cm^{-1} of acid-sonicated H-CNFs corresponded to the deformation vibration (out-of-plane) of O–H and the stretching vibration of the C–O carboxyl group, respectively. These bands appear at higher wavenumbers and indicate the presence of a dimer carboxyl, or more specifically, the bands at 1398 cm^{-1} and 1550 cm^{-1} with a shoulder were assigned to the stretching vibration of the carboxylate anion. The band at 1720 cm^{-1} was assigned to the stretching vibration of the carboxyl C=O group. It was also confirmed that the band between 3120 and 3450 cm^{-1} corresponded to the stretching vibration of the carboxyl O–H group. Thus, the edges of the graphene-hats were modified by carboxyl groups following sonication in a H_2SO_4–HNO_3 mixed acid solution.

Figure 4 shows SEM images (left) and corresponding size distributions (right) of H-CNFs separated using polycarbonate membrane filters with

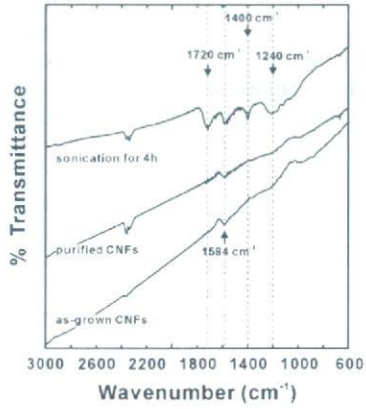

FIGURE 3. IR spectra of H-CNFs. From bottom: as-grown, purified, and cut H-CNFs.

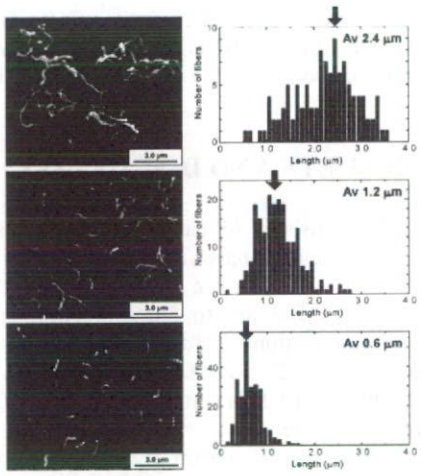

FIGURE 4. SEM images of cake on a filter (left) and corresponding size-distributions (right) of separated H-CNFs.

cylindrical pore diameters of 2.0, 1.2 and 0.4 μm, respectively. As a result of fitting the distribution histograms using a Gaussian function, the average length of nanofibers within the cake deposited on polycarbonate membrane filters with cylindrical pore diameters of 2.0, 1.2 and 0.4 μm was 2.4 μm, 1.2 μm and 0.6 μm, respectively. The yield of separated H-CNFs with lengths of 2.4 μm, 1.2 μm and 0.6 μm was 12.8, 26.7 and 35.9%, respectively. The residual 24.6% consisted of filtrate material and some losses resulting from the size-separation procedure.

The stability of acid-treated H-CNFs was determined by measuring the dispersion concentration *versus* the sediment time in distilled water or phosphate buffered saline (PBS) and is shown in Fig. 5. A calibration curve was constructed for the absorbance at 261 nm and the dispersed amount (mg mL^{-1}). These parameters showed a linear relationship in the range 0.001–0.1 mg mL^{-1}. These water-soluble H-CNFs were well dispersed in distilled water even after 500 hrs had elapsed (Fig. 5a). However, the stability of H-CNFs at 0.1 mg mL^{-1} gradually decreased. After 120 hrs, the concentration was reduced to 0.05 mg mL^{-1}. Finally, the concentrations of water-soluble H-CNFs with lengths of 0.6, 1.2 and 2.4 μm were reduced to the range 0.02–0.03 mg mL^{-1} after 500 hrs. Sedimentation is related to the ratio of the amount of hydrophilic group per surface area and their own weight and length. H-CNFs do not possess a hollow structure like CNTs, but a closed packing graphene-hat structure. H-CNFs are less stable than carbon nanotubes due to the larger density of H-CNFs. Meanwhile, the sediment effect was more rapid in the case of PBS. A concentration of 0.1 mg mL^{-1} gradually decreased to 0.05 mg mL^{-1} after 60 hrs.

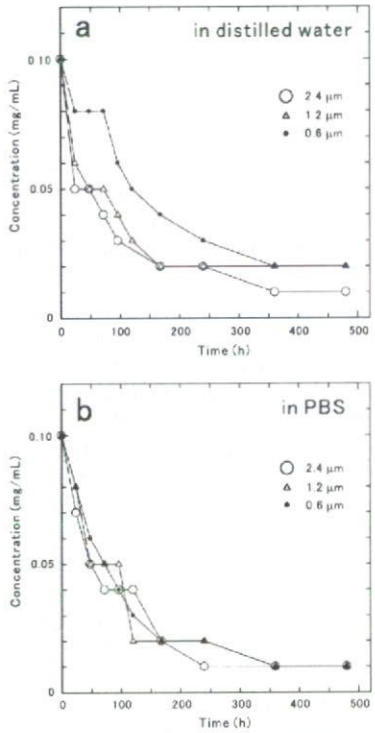

FIGURE 5. Stability of size-separated CNFs in distilled water (a) and PBS (b).

After 350 hrs, the concentration was reduced even further to 0.01 mg mL^{-1} in PBS (Fig. 5b). M. Sano *et al.* reported that single-walled carbon nanotubes (SWCNTs) modified with carboxyl groups aggregated when the concentration of SWCNTs reached a critical coagulation concentration (*ccc*) [11]. As each ion concentration in PBS that contains Na^+ (152 mM), K^+ (4.1 mM), Mg^{2+} (1.1 mM) and Ca^{2+} (0.9 mM) is higher than the *ccc* except for K^+ (26 mM), we speculated that H-CNFs would easily form sediments. These results might also indicate that H-CNFs form sediments in nutrient medium and living organisms, where ion concentrations are similar to those of PBS.

CONCLUSIONS

Hat-stacked carbon nanofibers (H-CNFs) were size-separated using a multi-step microfiltration process employing polycarbonate membrane filters with respective cylindrical pore diameters of 2.0, 1.2 and 0.4 μm. The average length of separated H-CNFs was 2.4 μm, 1.2 μm and 0.6 μm, respectively, and the yield of separated H-CNFs with lengths of 2.4 μm, 1.2 μm and 0.6 μm was 12.8, 26.7 and 35.9%, respectively. These water-soluble H-CNFs were dispersed in distilled water and PBS even after 500 hrs had elapsed. The stability of H-CNFs at 0.1 mg mL^{-1} gradually